Thermal Process Maps for Controlling Microstructure in Laser-Based Solid Freeform Fabrication

S. Bontha and N.W. Klingbeil
Department of Mechanical and Materials Engineering
Wright State University
Dayton, OH, 45435

Abstract

The ability to predict and control microstructure in laser deposited materials requires an understanding of the thermal conditions at the onset of solidification. The focus of this work is the development of thermal process maps relating solidification cooling rate and thermal gradient (the key parameters controlling microstructure) to laser deposition process variables (laser power and velocity). The approach employs the well-known Rosenthal solution for a moving point heat source traversing an infinite substrate. Cooling rates and thermal gradients at the onset of solidification are numerically extracted from the Rosenthal solution throughout the depth of the melt pool, and dimensionless process maps are presented for both thin-wall (2-D) and bulky (3-D) geometries. In addition, results for both small-scale (LENS^{TM}) and large-scale (higher power) processes are plotted on solidification maps for predicting grain morphology in Ti-6Al-4V. Although the Rosenthal results neglect temperature-dependent properties and latent heat effects, a comparison with 2-D FEM results over a range of LENS^{TM} process variables suggests that they can provide reasonable estimates of trends in solidification microstructure. The results of this work suggest that changes in process variables could potentially result in a grading of the microstructure (both grain size and morphology) throughout the depth of the deposit, and that the size-scale of the laser deposition process is important.

Introduction

Laser deposition of titanium alloys and other metallic materials is currently under consideration for application to aerospace components, and offers significant increases in efficiency and flexibility compared to conventional manufacturing methods [1]. However, the widespread use of this promising technology will ultimately depend on the ability to predict and control the microstructure and resulting mechanical properties of the deposit [2]. To date, only limited experimental data exists to link deposition process variables (e.g., laser power and velocity) to resulting microstructure (e.g., grain size and morphology) in laser deposited titanium alloys [3-5], and suitable microstructures have typically been obtained only by trial and error. The ability to predict and control microstructure in laser deposition processes requires an understanding of the thermal conditions at the onset of solidification, which is the focus of this work.

Recent studies in the literature [6-10] have employed the Rosenthal solution [11] for a moving point heat source on an infinite substrate to identify the dimensionless process variables governing thermal conditions in laser deposition processes. In conjunction with thermal finite element modeling, this has enabled the development of "process maps" relating deposition process variables to melt pool size and residual stress in both thin-wall (2-D) and bulky (3-D) geometries. In the current study, a similar approach is used to investigate solidification cooling rates and thermal gradients (the key parameters controlling microstructure) in laser deposition processes. Cooling rates and thermal gradients at the onset of solidification are numerically

extracted from the Rosenthal solution throughout the depth of the melt pool, and dimensionless process maps are developed for both thin-wall and bulky deposits. The results are plotted on solidification maps for Ti-6Al-4V, which provide insight into the effects of process variables on grain morphology. Finally, a comparison is made between small-scale processes (e.g., LENS™) and large-scale (higher power) processes, several of which are under development for laser additive manufacturing applications. This comparison is particularly relevant in light of other recent investigations into the effects of size-scale on melt pool size and residual stress [12].

Geometries Considered

This study considers both the thin-wall (2-D) and bulky (3-D) geometries of Fig. 1, in which the process variables of interest are the absorbed laser power αQ and velocity V. In each case, it is assumed that the height h and length L are sufficiently large such that the steady-state Rosenthal solution for a point heat source traversing an infinite half-space applies [11].

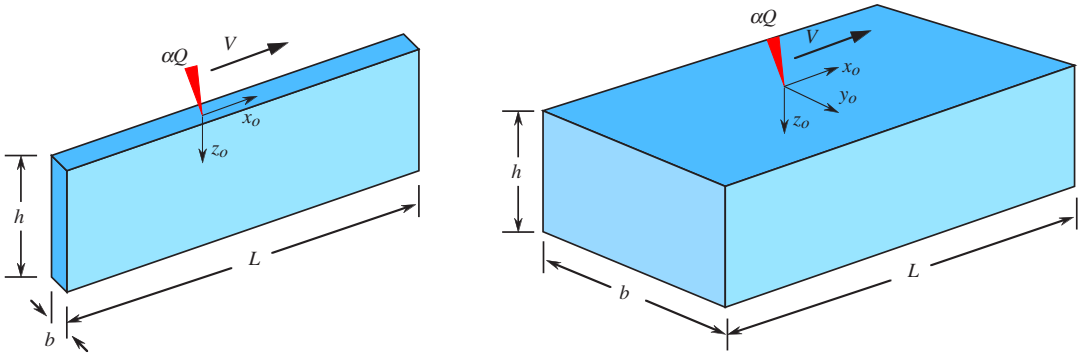

Figure 1. a) Thin-Wall (2-D) and b) Bulky (3-D) Geometries Considered

Thermal Process Maps for Thin-Wall Geometries

The results of this section are limited to the thin-wall geometry of Fig. 1a. Such structures are commonly manufactured using LENS™ and other small-scale metal deposition processes. As discussed by Vasinonta *et al.* [8], the 2-D Rosenthal point source solution for the geometry of Fig. 1a can be expressed in dimensionless form as

$$\bar{T} = e^{-\bar{x}_o} K_o\left(\sqrt{\bar{x}_o^2 + \bar{z}_o^2}\right), \tag{1}$$

where K_o is the modified Bessel function of the second kind, order zero. The dimensionless variables in eq. (1) are defined in terms of the absorbed laser power αQ and velocity V as

$$\bar{T} = \frac{T - T_o}{\alpha Q / \pi k b}, \quad \bar{x}_o = \frac{x_o}{2k / \rho c V} \quad \text{and} \quad \bar{z}_o = \frac{z_o}{2k / \rho c V}, \tag{2}$$

where T is the temperature at a location (x_o,z_o) relative to the moving point source (see Fig. 1a), T_o is the initial temperature of the wall, b is the wall thickness, and ρ, c and k are the density, specific heat and thermal conductivity of the material, respectively.

As previously discussed, the parameters of interest in controlling microstructure are the solidification cooling rate and thermal gradient. Noting that the relative coordinates (x_o,z_o) at any time t are related to any fixed spatial coordinates (x,z) as $(x_o,z_o) = (x\text{-}Vt,z)$, expressions for the

dimensionless cooling rate and thermal gradient can be obtained through differentiation of eq. (1). In so doing, the dimensionless cooling rate and thermal gradient are defined as

$$\frac{\partial \overline{T}}{\partial \overline{t}} = \left(\frac{2\pi k^2 b}{\alpha Q \rho c V^2} \right) \frac{\partial T}{\partial t}, \quad \left| \overline{\nabla T} \right| = \left(\frac{2\pi k^2 b}{\alpha Q \rho c V} \right) \left| \nabla T \right|. \tag{3}$$

Values of the dimensionless cooling rate and thermal gradient at the onset of solidification are obtained by evaluating the corresponding derivatives of eq. (1) along the boundary of the melt pool. The coordinates (x_o,z_o) which lie on the boundary of the melt pool are obtained by replacing T with the melting point T_m and finding the roots of eq. (1) numerically. The numerical root finding was conducted using the software package MATLAB, and results for melt pool length were verified against those previously published in the literature [6-10].

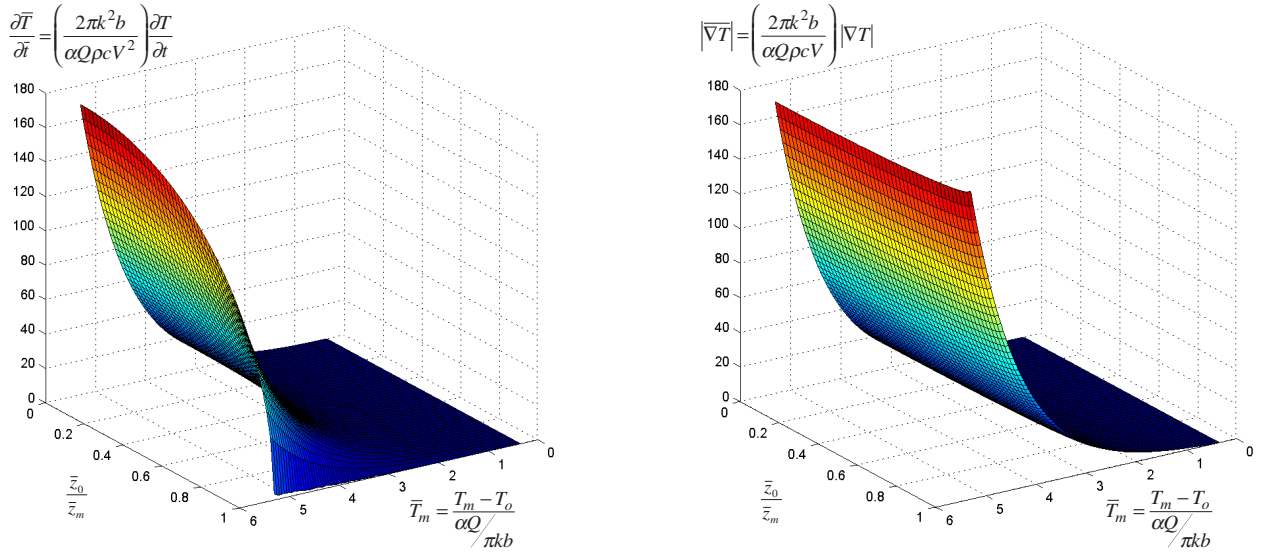

a) b)

Figure 2. Process Maps for Solidification a) Cooling Rate and b) Thermal Gradient for Thin-Wall Geometries

In conjunction with the dimensionless variables defined in eqs. (2) and (3), the Rosenthal solution enables the development of process maps for solidification cooling rate and thermal gradient throughout the depth of the melt pool. Such results are shown in Fig. 2, where the dimensionless cooling rate and thermal gradient are plotted as a function of normalized melting temperature $\overline{T}_m$ and relative depth within the melt pool $\bar{z}_o / \bar{z}_m$. The normalized melting temperature varies with laser power, and is defined in terms of the melting temperature T_m as

$$\overline{T}_m = \frac{T_m - T_o}{\alpha Q / \pi k b}. \tag{4}$$

The normalized depth varies in the range $0 \le \bar{z}_o / \bar{z}_m \le 1$, where $\bar{z}_m$ signifies the deepest extent of the melt pool for a given value of $\overline{T}_m$.

The results of Fig. 2 indicate that for fixed material properties, changes in laser power (or changes in $\overline{T}_m$) can have a significant effect on the solidification cooling rate and thermal

gradient. When plotted on a log scale (not shown here), the results indicate that changes in laser power can change both the dimensionless cooling rate and thermal gradient by several orders of magnitude. Furthermore, for fixed values of $\overline{T}_m$ (or fixed laser power), the normalizations of eq. (3) indicate that the actual thermal gradient scales linearly with the laser velocity, while the actual cooling rate scales with the square of the velocity. Hence, changes in laser velocity can also have a significant effect on solidification cooling rate and thermal gradient. Finally, the results of Fig. 2 suggest that for fixed laser power and velocity, the cooling rate can vary significantly throughout the depth of the melt pool, particularly for high values of $\overline{T}_m$. On the other hand, the thermal gradient is more sensitive to depth within the melt pool for low values of $\overline{T}_m$. These results suggest that depending on the material system considered, changes in laser power might allow grading of the microstructure as a function of depth within the deposit.

Thermal Process Maps for Bulky 3-D Geometries

As discussed by Vasinonta *et al.* [9], the Rosenthal solution for a point heat source traversing the top of a bulky 3-D geometry (Fig. 1b) can be expressed in dimensionless form as

$$\overline{T} = \frac{e^{-\left(\bar{x}_0 + \sqrt{\bar{x}_0^2 + \bar{y}_0^2 + \bar{z}_0^2}\right)}}{2\sqrt{\bar{x}_0^2 + \bar{y}_0^2 + \bar{z}_0^2}}, \tag{5}$$

where

$$\overline{T} = \frac{T - T_0}{\left(\alpha Q / \pi k\right)\left(\rho c V / 2k\right)},\ \bar{x}_o = \frac{x_o}{2k/\rho c V},\ \bar{y}_o = \frac{y_o}{2k/\rho c V} \text{ and } \bar{z}_o = \frac{z_o}{2k/\rho c V}. \tag{6}$$

Comparison of eqs. (6) and (2) reveals that in terms of laser deposition process variables, the temperature normalization for bulky 3-D geometries is different from that for thin-wall geometries. The 2-D normalization is a function only of laser power, while the 3-D normalization depends on both laser power and velocity. The dimensionless cooling rate and thermal gradient for bulky 3-D geometries are defined as

$$\frac{\partial \overline{T}}{\partial \bar{t}} = \left(\frac{2k}{\rho c V}\right)^2 \left(\frac{\pi k}{\alpha Q V}\right) \frac{\partial T}{\partial t},\quad \left|\overline{\nabla T}\right| = \left(\frac{2k}{\rho c V}\right)^2 \left(\frac{\pi k}{\alpha Q}\right) \left|\nabla T\right|. \tag{7}$$

The above definitions have a higher order velocity dependence compared to the 2-D normalizations of eq. (3), which is a direct result of the temperature normalization of eq. (6).

For bulky 3-D geometries, values of the dimensionless cooling rate and thermal gradient at the onset of solidification are obtained by evaluating the corresponding derivates of eq. (5) along the boundary of the melt pool cross section in the (x,z) plane (i.e., along y_o = 0). The resulting process maps for solidification cooling rate and thermal gradient are plotted in Fig. 3 as a function of normalized melting temperature $\overline{T}_m$ and relative depth within the melt pool $\bar{z}_o / \bar{z}_m$. Note that according to eq. (6), the dimensionless melting temperature for bulky 3-D geometries is defined in terms of both laser power and velocity as

$$\overline{T}_m = \frac{T_m - T_o}{\left(\alpha Q / \pi k\right)\left(\rho c V / 2k\right)}. \tag{8}$$

The results of Fig. 3 indicate that for fixed material properties, changes in laser power or velocity (or changes in $\overline{T}_m$) can have a significant effect on cooling rate and thermal gradient, and hence the resulting microstructure. In general, the trends are similar to those for thin-wall geometries (Fig. 2). However, owing to the different temperature normalizations in 2-D and 3-D, comparing the magnitudes of the dimensionless results in Figs. 2 and 3 can be misleading. For example, although the magnitudes of the *dimensionless* cooling rates are larger in Fig. 2a than in Fig. 3a, the *actual* cooling rate for a given laser power and velocity is greater in 3-D than in 2-D.

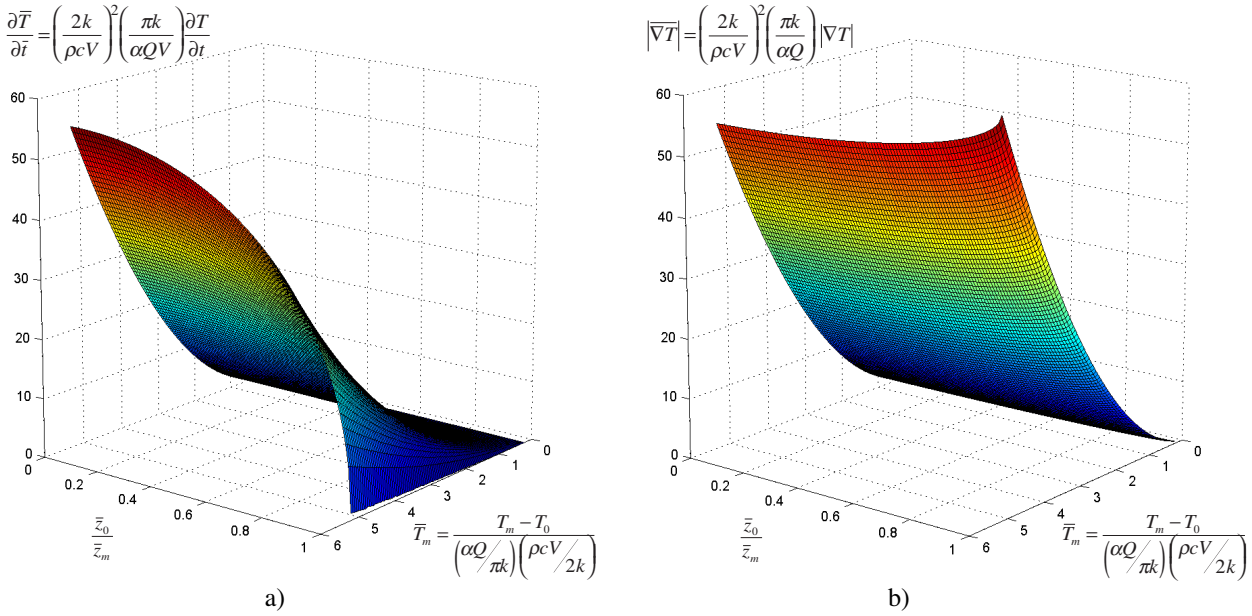

a) b)

Figure 3. Process Maps for Solidification a) Cooling Rate and b) Thermal Gradient for Bulky (3-D) Geometries

Solidification Maps for Ti-6Al-4V

As discussed in [2,3], results for solidification thermal gradient and cooling rate can be interpreted in the context of a solidification map to provide predictions of grain morphology in laser-deposited Ti-6Al-4V. Given the solidification cooling rate $\partial T / \partial t$ and thermal gradient $G = \left|\nabla T\right|$, the solidification velocity R is determined as

$$R = \frac{1}{G}\frac{\partial T}{\partial t}. \tag{9}$$

The expected grain morphology can be predicted as either equiaxed, columnar or mixed by plotting points in G vs. R space (i.e., on the "solidification map"), which has been previously calibrated for Ti-6Al-4V [3].

Solidification maps showing the effects of laser power and velocity over a range of typical LENS™ process variables for thin-wall Ti-6Al-4V deposits are shown in Figures 4 and 5. The results of Figs. 4a and 5a have been extracted from 2-D thermal FEM analyses of a

particular thin-wall geometry (b=2.26 *mm*, h=8.69 *mm*, L=50.4 *mm*), as described by Klingbeil *et al*. [2]. The FEM results include temperature-dependent properties and latent heat effects for Ti-6Al-4V. The results of Figs. 4b and 5b are extracted directly from the Rosenthal results of Fig. 2, with thermophysical properties for Ti-6Al-4V assumed constant at the melting temperature T_m=1654°*C*. Both the FEM and Rosenthal results assume the fraction of absorbed laser power to be α=0.35.

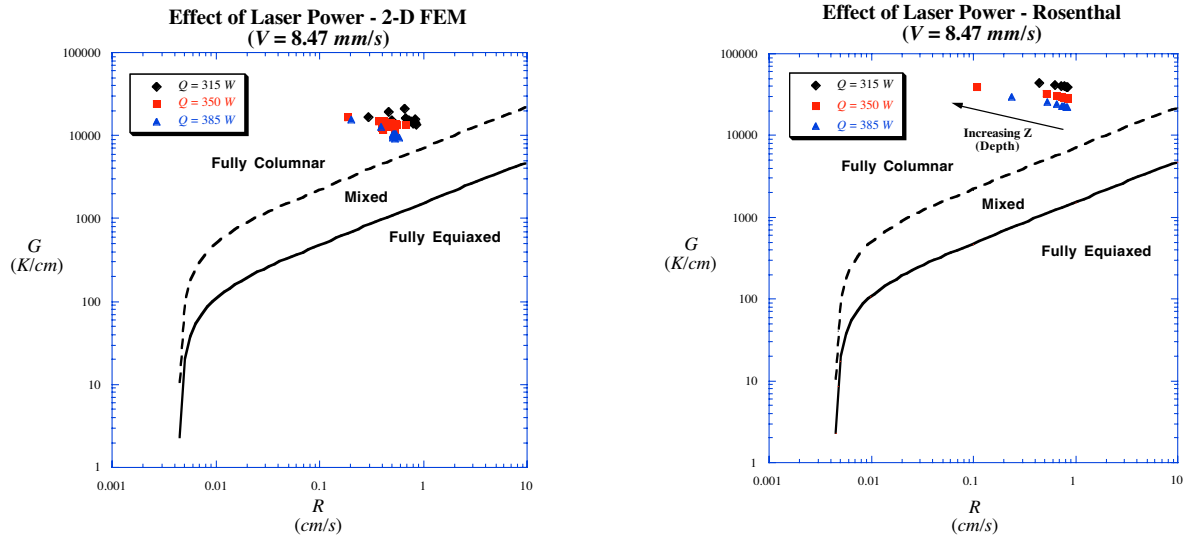

a) b)

Figure 4. Effect of Laser Power on Grain Morphology from a) 2-D FEM and b) 2-D Rosenthal Solution

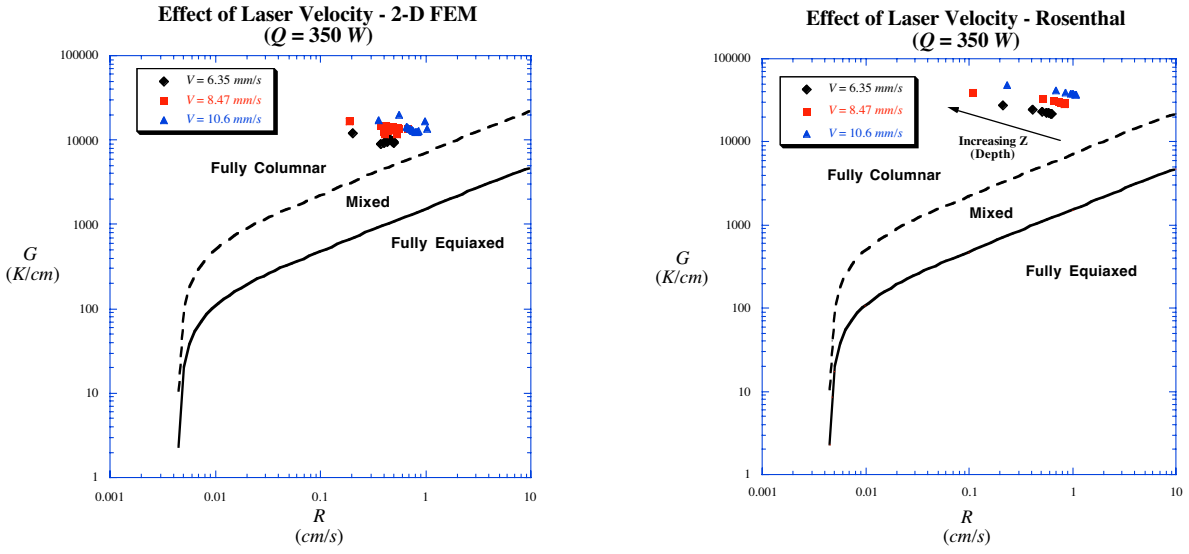

a) b)

Figure 5. Effect of Laser Velocity on Grain Morphology from a) 2-D FEM and b) 2-D Rosenthal Solution

Although the Rosenthal results neglect the nonlinear effects of temperature-dependent properties and latent heat of transformation, trends in G vs. R data are in reasonably good agreement with the FEM results. In particular, both the Rosenthal and FEM results predict a fully columnar morphology, which is in keeping with experimental observations of LENS™ deposited Ti-6Al-4V [3-5]. However, results also suggest that increasing laser incident energy

(increasing power or decreasing velocity) tends to shift the data closer to the boundary for a mixed columnar/equiaxed grain morphology.

Given the utility of the Rosenthal results for thin-wall LENS™ deposits, the approach can be extended to provide insight into large-scale (higher power) processes. Since wall thickness is an unknown function of laser power, a comparison between LENS™ and large-scale processes is best made for bulky 3-D geometries. Solidification maps obtained from the 3-D Rosenthal results throughout the depth of the melt pool are plotted in Fig. 6 for both small-scale (LENS™) and large-scale processes. The range of LENS™ powers is restricted to 350-850 *W*, while large-scale processes are considered in the range 5000-30000 *W*. In each case, the laser velocity is held constant at $V = 8.47$ *mm/s*, and the fraction of absorbed laser power is taken to be α=0.35.

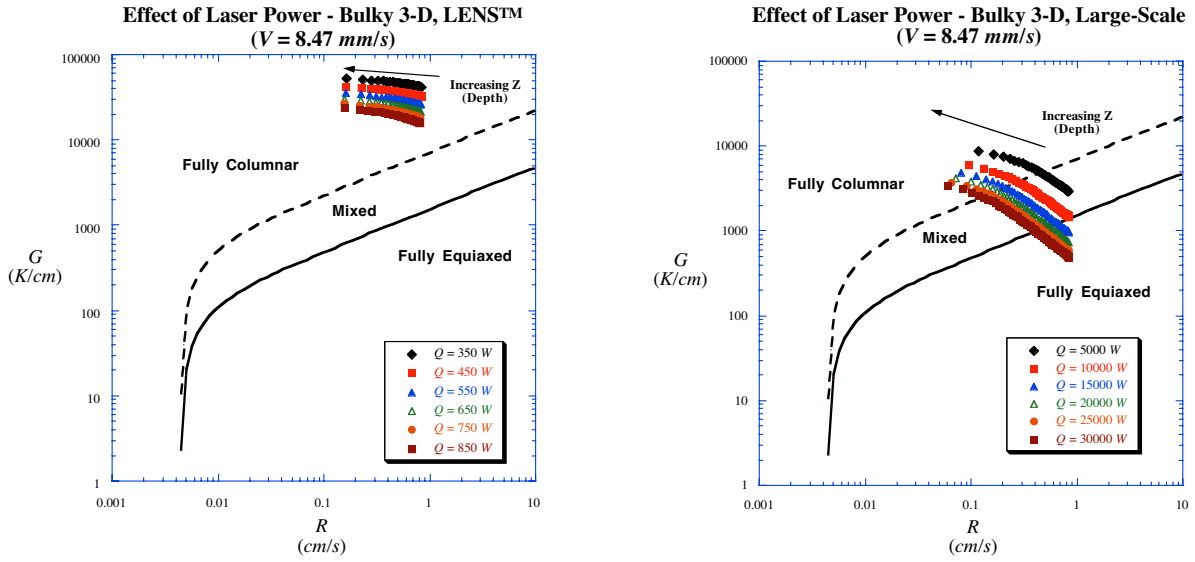

a) b)

Figure 6. Predicted Grain Morphology in Bulky 3-D Deposits for a) Small-Scale (LENS™) and b) Large-Scale Processes

The results of Fig. 6 reveal that size-scale can have a significant effect on predicted grain morphology in laser deposited Ti-6Al-4V. The results of Fig. 6a predict a fully columnar morphology over the full range of LENS™ powers, which is in keeping with experimental observations [3]. However, the results of Fig. 6b reveal that large-scale processes can result in a grading of the microstructure throughout the depth of the deposit, with a mixed or even fully-equiaxed microstructure at the surface. As observed for thin-wall deposits, the trend toward mixed or equiaxed microstructure increases with laser incident energy.

Conclusions

The ability to predict and control microstructure in laser deposited materials requires an understanding of the thermal conditions at the onset of solidification, which is the focus of this work. Based on the Rosenthal solution for a moving point heat source, process maps for solidification cooling rate and thermal gradient are presented as a function of deposition process variables and depth within the deposit. The results of this work suggest that variations in laser power and velocity can change solidification cooling rates and thermal gradients by several orders of magnitude, which depending on the material system could have a significant effect on resulting microstructure and mechanical properties. Results specifically for Ti-6Al-4V suggest

that increases in laser incident energy could potentially yield a mixed or even fully-equiaxed microstructure near the surface of the deposit, and that the size-scale of the process is important.

Acknowledgments

This work has been supported by the National Science Foundation, grant number DMI-0224517, as well as by the Joint AFRL/DAGSI Research Program, project number ML-WSU-01-11. The authors would also like to thank J.L. Beuth, P.A. Kobryn and H.L. Fraser for their thoughts and insights regarding this collaborative research effort.

References

1. Kobryn, P.A. and Semiatin, S.L., 2001, "The Laser Additive Manufacture of Ti-6Al-4V," *JOM*, Vol. 53, No. 9, pp. 40-42.

2. Klingbeil, N.W., Brown, C.J., Bontha, S., Kobryn, P.A. and Fraser, H.L., 2002, "Prediction of Microstructure in Laser Deposition of Titanium Alloys," *Solid Freeform Fabrication Proceedings*, (D.L. Bourell, R. H. Crawford, J.J. Beaman, K.L. Wood, H.L. Marcus, eds.), Austin, August 2002, pp. 142-149.

3. Kobryn, P.A., Moore, E.H. and Semiatin, S.L., 2000, "The Effect of Laser Power and Traverse Speed on Microstructure, Porosity and Build Height in Laser-Deposited Ti-6Al-4V," *Scripta Materiala,* Vol. 43, pp. 299-305.

4. Kobryn, P.A. and Semiatin, S.L., 2001, "Mechanical Properties of Laser-Deposited Ti-6Al-4V," *Solid Freeform Fabrication Proceedings*, (D.L. Bourell, J.J. Beaman, R.H. Crawford, H.L. Marcus and J.W. Barlow, eds.), Austin, August 2001.

5. C. A. Brice, K. I. Schwendner, D. W. Mahaffey, E. H. Moore, and H. L. Fraser, 1999, "Process Variable Effects On Laser Deposited Ti-6Al-4V," *Solid Freeform Fabrication Proceedings*, (D.L. Bourell, J.J. Beaman, R.H. Crawford, H.L. Marcus and J.W. Barlow, eds.), Austin, August 1999.

6. Vasinonta, A., Beuth, J.L. and Griffith, M.L.,1999, "Process Maps for Laser Deposition of Thin-Walled Structures," *Solid Freeform Fabrication Proceedings*, (D.L. Bourell, J.J. Beaman, R.H. Crawford, H.L. Marcus and J.W. Barlow, eds.), Austin, August 1999, pp. 383-391.

7. Vasinonta, A., Beuth, J.L. and Griffith, M.L., 2000, "Process Maps for Controlling Residual Stress and Melt Pool Size in Laser-Based SFF Processes," *Solid Freeform Fabrication Proceedings*, (D.L. Bourell, J.J. Beaman, R.H. Crawford, H.L. Marcus and J.W. Barlow, eds.), Austin, August 2000, pp. 200-208.

8. Vasinonta, A., Beuth, J.L. and Griffith, M.L., 2001, "A Process Map for Consistent Build Conditions in the Solid Freeform Fabrication of Thin-Walled Structures," *Journal of Manufacturing Science and Engineering*, Vol. 123, No. 4, pp. 615-622.

9. Vasinonta, A., Beuth, J.L., and Ong, R., 2001, "Melt Pool Size Control in Thin-Walled and Bulky Parts via Process Maps," Solid Freeform Fabrication Proceedings (D.L. Bourell, J.J. Beaman, R.H. Crawford, H.L. Marcus, K.L. Wood and J.W. Barlow, eds.), Proc. 2001 Solid Freeform Fabrication Symposium, Austin, August 2001, pp. 432-440.

10. Beuth, J.L. and Klingbeil, N.W., 2001, "The Role of Process Variables in Laser-Based Direct Metal Solid Freeform Fabrication," *JOM*, Vol. 53, No. 9, pp. 36-39.

11. Rosenthal, D., 1946, "The Theory of Moving Sources of Heat and its Application to Metal Treatments," *Transactions of ASME*, Vol. 68, pp. 849-866.

12. Birnbaum, A., Aggarangsi, P. and Beuth, J., 2003, "Process Scaling and Transient Melt Pool Size Control in Laser-Based Additive Manufacturing Processes," *Solid Freeform Fabrication Proceedings*, Austin, August 2003.